



# On the performance and mechanisms of toluene removal by FeO<sub>x</sub>/SBA-15-assisted non-thermal plasma at atmospheric pressure and room temperature

Meijuan Lu<sup>a</sup>, Rong Huang<sup>a</sup>, Junliang Wu<sup>a,b</sup>, Mingli Fu<sup>a,b</sup>, Limin Chen<sup>a,b</sup>, Daiqi Ye<sup>a,b,\*</sup>

<sup>a</sup> College of Environment and Energy, South China University of Technology, Guangzhou 510006, China

<sup>b</sup> Guangdong Provincial Key Laboratory of Atmospheric Environment and Pollution Control (SCUT), Guangzhou 510006, China

## ARTICLE INFO

### Article history:

Received 13 May 2014

Received in revised form 6 July 2014

Accepted 10 July 2014

Available online 10 August 2014

### Keywords:

Dielectric barrier discharge

Toluene removal

Catalyst of FeO<sub>x</sub>/SBA-15

Oxygen species

## ABSTRACT

FeO<sub>x</sub>/SBA-15 catalysts were prepared via impregnation and utilized for toluene removal in dielectric barrier discharge (DBD) plasma at atmospheric pressure and room temperature. Toluene removal was investigated in the environment of various mixed N<sub>2</sub>/O<sub>2</sub> plasmas, showing that toluene removal efficiency and CO<sub>x</sub> selectivity were greatly increased by FeO<sub>x</sub>/SBA-15 and that the organic intermediates were greatly reduced by catalysts. In pure N<sub>2</sub> plasma, the bulk oxygen in the catalyst was involved in the toluene oxidation, and the 3%FeO<sub>x</sub>/SBA-15 catalyst showed the optimal toluene oxidation activity. The catalysts were characterized by scanning electron microscopy (SEM), X-ray diffraction (XRD), N<sub>2</sub> adsorption-desorption, X-ray photoelectron spectroscopy (XPS), H<sub>2</sub> temperature-programmed reduction (H<sub>2</sub>-TPR) and O<sub>2</sub> temperature-programmed desorption (O<sub>2</sub>-TPD), showing that toluene oxidation was closely related to the highly dispersed nature of iron on the SBA-15 surface, the reduction temperature of Fe<sup>2+</sup> and the oxygen adsorption ability of the catalyst. The pathways of toluene decomposition in the combination of FeO<sub>x</sub>/SBA-15 with a non-thermal plasma (NTP) system were proposed based on the identified intermediates.

© 2014 Elsevier B.V. All rights reserved.

## 1. Introduction

Volatile organic compounds (VOCs), as chief atmospheric pollution precursors, are harmful to humans and the environment [1]. The toluene is a typical VOC in that it is emitted in high levels and difficult to abate [2]. Consequently, considerable attention has been paid to the development of methods for its removal. Recently, NTP technology has emerged as a promising method [3–11]. However, it also suffers from high energy consumption and incomplete oxidization, and the process is difficult to control [12,13]. To overcome these problems, the used of a catalyst has been coupled with NTP [14–16], wherein the VOCs removal rate increases with the assistance of adsorption [17]. Considering the importance of adsorption, various porous materials, such as γ-Al<sub>2</sub>O<sub>3</sub> and molecular sieves, have been studied [18–20]. The mesoporous material SBA-15 shows relatively high adsorption for toluene because of

its special micropore structure [20]. Thus, the residence time of toluene can be further increased if SBA-15 is added into the plasma system. However, SBA-15 is chemically inert for various catalytic applications because of its lack of acid and redox sites [21]. The incorporation of metal is an efficient method to improve the catalysis properties of this material. Among the various metal oxides, iron oxide has received extensive attention due to its relatively low cost, high activity, and environmental friendliness [22,23] as well as the O<sub>2</sub> transportation via facile interconversion between Fe<sup>2+</sup> and Fe<sup>3+</sup> states [24]. Our previous work has also disclosed the outstanding performance of FeO<sub>x</sub> for toluene degradation in DBD plasma [25]. Therefore, it is vital to incorporate iron into SBA-15 material for VOCs plasma-catalysis oxidation because of the contrasting characteristics of these two materials. However, at present, the application of NTP coupled with FeO<sub>x</sub>/SBA-15 catalysis in toluene degradation is scarce in the literature.

Oxygen species serve as an oxidizing agent to scavenge the VOCs and form carbon oxides. Their two main sources are gas-phase oxygen in the feed gas stream and bulk-phase oxygen in the catalyst. The gas-phase oxygen can be dissociated into atomic oxygen by discharge [26], and can promote the decomposition of CF<sub>4</sub> into CO<sub>x</sub> in air thermal plasmas [27]. Previous research shows

\* Corresponding author at: College of Environment and Energy, South China University of Technology, Guangzhou Higher Education Mega Centre, Panyu District, Guangzhou 510006, China. Tel.: +86 20 39380516; fax: +86 20 39380518.

E-mail address: [cedqye@scut.edu.cn](mailto:cedqye@scut.edu.cn) (D. Ye).

that the decomposition efficiency of benzene increases with the O<sub>2</sub> partial pressures [28]. However, the catalysts, especially transition metal oxides, generally contain lattice oxygen, surface oxygen and adsorbed oxygen [29,30]. Regardless of type, all oxygen in the catalyst can be described as the bulk-phase oxygen of the catalyst, which can also oxidize VOCs into CO<sub>x</sub> in the plasma [31,32]. Herein, gas-phase oxygen in the feed gas stream and bulk-phase oxygen in the catalyst are both expected to play important roles during VOC removal.

In this work, iron loaded on SBA-15 was selected as a catalyst to oxidize toluene (100 ppm) in various mixed N<sub>2</sub>/O<sub>2</sub> plasmas at atmospheric pressure and room temperature. To better understand the structure and possible metal-support interaction of the iron oxide species and SBA-15 support, the catalysts were characterized by SEM, XRD, N<sub>2</sub> adsorption-desorption, XPS, H<sub>2</sub>-TPR and O<sub>2</sub>-TPD. The organic by-products of toluene oxidation were identified to provide a better understanding of the VOC oxidation mechanism over FeO<sub>x</sub>/SBA-15 catalysts.

## 2. Experimental

### 2.1. Experimental setup

**Fig. 1** shows a schematic diagram of the experimental arrangement designed for toluene removal via the combination of a catalyst with plasma. The toluene used was obtained by bubbling toluene with a N<sub>2</sub> gas stream in a bubbler. High-purity N<sub>2</sub> (99.99%) was divided into two streams. The first stream was allowed to pass through the pure toluene liquid (99.5%) (Guangzhou Chemical Reagent, China) kept in an ice and water bath (0 °C) to produce the toluene vapor. The second stream was mixed with high-purity O<sub>2</sub> (99.99%) in a mixing chamber. The combined stream was then mixed with vaporized toluene in another mixing chamber. The gas flow rates were adjusted and controlled using mass flow controllers (MFCs) (Seven Star Co., China). The mixture was introduced into the reactor at a flow rate of 300 mL/min, with an initial toluene concentration of 100 ppm and a gas residence time of 0.45 s. All of the gases used in this study were purchased from Guangzhou Jun Qi Gas Co., Ltd.

Toluene oxidation was carried out in a fixed-bed flow reactor that containing 0.2 g of the catalyst (40–60 mesh) and 1.6 g of silica sand (40–60 mesh). All of the experiments in the discharge stages were conducted at atmospheric pressure and room temperature. The gas leaving the reactor was analyzed using an online gas chromatograph (GC2014C, Shimadzu) equipped with two FID detectors; one for organic compounds, featuring a TG-BOND Q column (30 m, 0.32 mm) (60 °C), and one, equipped with a methanizer, for carbon monoxide and carbon dioxide analysis using a 5 A molecular sieve (2 m, 2 mm) and Poraplot Q column (4 m, 2 mm) (60 °C).

The organic by-products (gas phase) were preconcentrated by active carbon placed downstream of the NTP reactor, and then the active carbon was dispersed into the CS<sub>2</sub> solution (Chromatographic Grade) under ultrasonic vibration for 120 min. The supernatant was filtered with a 0.22-μL filter membrane and analyzed by a GC-MS (QP2010, Shimadzu) using an Rtx-5MS capillary column. The column temperature was 40 °C for the first 2 min and was then increased to 220 °C at 6 °C/min, where it was maintained for 5 min. The MS detector was run in scan mode with a mass range of 45–450 amu. The electron ionization (EI) method was used. MS identification was conducted using the NIST 08 databank (NIST/EPA/NIH Mass Spectral Library). The organic by-products on the catalyst surface were analyzed using the same procedure.

The toluene removal was expressed as follows:

$$\text{toluene removal efficiency (\%)} = \frac{C_0 - C}{C_0} \times 100\%$$

$$\text{CO}_2 \text{ selectivity (\%)} = \frac{C_{\text{CO}_2}}{7(C_0 - C)} \times 100\%$$

$$\text{CO}_x \text{ selectivity (\%)} = \frac{C_{\text{CO}_x}}{7(C_0 - C)} \times 100\%$$

where C<sub>0</sub> and C are the initial and final concentrations of toluene, C<sub>CO<sub>2</sub></sub> is the outlet concentration of CO<sub>2</sub> and C<sub>CO<sub>x</sub></sub> is the sum of the outlet concentrations of CO and CO<sub>2</sub>. All concentrations are units of ppm and the data were recorded by an online gas chromatograph after the plasma starting for 30 min, which was a stabilized state for toluene removal.

### 2.2. Plasma system

The cylinder reactor was made of quartz glass, with a length of 180 mm, inner diameter of 10 mm and wall thickness of 1 mm. The quartz cylinder was wrapped by copper wire as the ground electrode, delimiting the length of the discharge zone to 30 mm. A stainless-steel rod with a diameter of 2 mm was used as the inner electrode and was connected to an AC high-voltage power supply that varied from 0 to 15 kV at a frequency of 50 Hz, resulting in a discharge gap of 4 mm. The applied voltage and current of the reactor were measured by a high-voltage probe and a digital power meter. The discharge power was the product of the applied voltage and the current [14,33–35]. The SED was calculated from the following expression:

$$\text{SED (J/L)} = \frac{\text{discharge power (W)}}{\text{gas flow rate (L/s)}}$$

All of the experimental results were compared based on specific energy density (SED) in this investigation.

### 2.3. Catalyst preparation

Catalysts were prepared via impregnation using SBA-15 (Nanjing XFNANO Materials Tech Co., Ltd.) as the support and iron nitrate ethanol solution of the desired concentration as the precursor. The support was stirred in the iron solution for 24 h at room temperature, and the solvent was then removed by evaporation at 60 °C. The residue was dried at 120 °C for 12 h, and calcined at 500 °C for 4 h. The resulting catalysts contained 1%, 3% and 5% (wt.%) iron loading and were denoted as 1%FeO<sub>x</sub>/SBA-15, 3%FeO<sub>x</sub>/SBA-15 and 5%FeO<sub>x</sub>/SBA-15, respectively.

### 2.4. Catalyst characterization

SEM microphotographs were obtained with an S-3700N electron microscope (Hitachi, Japan) operating at 5.0 kV.

XRD patterns were collected using a D8 ADVANCE X-ray diffractometer (Bruker, Germany) with Ni-filtered Cu K $\alpha$  radiation ( $k=0.15418 \text{ nm}$ ) in the 2θ range of 0.6 to 5° and 5 to 90° at a scanning rate of 4° min<sup>-1</sup>. The X-ray tube was operated at 40 kV and 40 mA.

N<sub>2</sub> adsorption-desorption isotherms were measured at –196 °C using a Micromeritics ASAP 2020 system. The sample (0.1 g) was pretreated for 6 h at 300 °C in a vacuum system, and the Brunauer–Emmett–Teller (BET) equation (relative pressure between 0.06 and 0.20) was employed to calculate the specific surface areas. The pore size and pore volume were calculated from the adsorption branches of N<sub>2</sub> physisorption isotherms and the Barrett–Joyner–Halenda (BJH) model.

The composition of elements and their valences on the catalyst surface were analyzed by XPS using an ESCALAB 250 spectrometer (Thermo Fisher Scientific, USA) equipped with a hemispherical

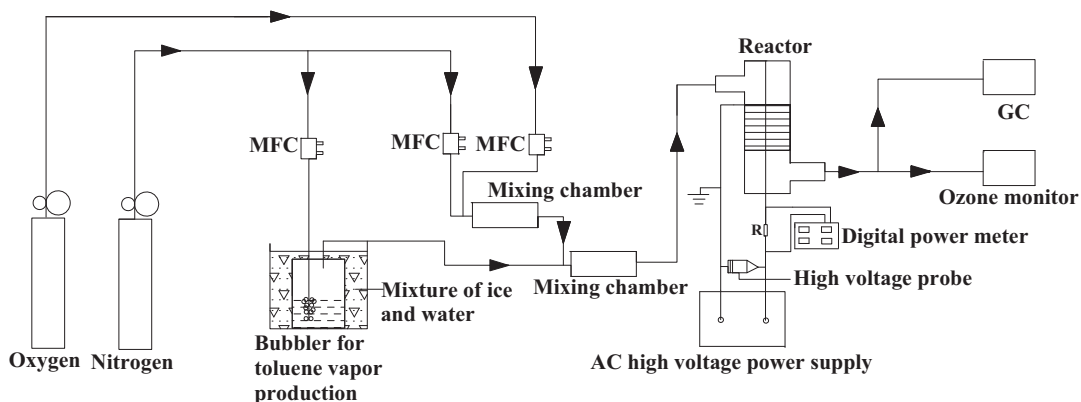


**Fig. 1.** Schematic of the experimental setup.

electron analyzer, employing a Mg K $\alpha$  radiation source (1253.6 eV) of 25 W. All binding energies were referenced to the C 1s line at 284.6 eV, which provided an accuracy of  $\pm 0.48$  eV within the full scanning range of 0 to 1100 eV. XPS peak 4.1 software was used for curve fitting.

H<sub>2</sub>-TPR analysis was performed on a Micromeritics AutoChem II 2920 instrument. First, 40 mg of the catalyst was pretreated at 300 °C using high-purity Ar (30 mL/min) for 30 min and then cooled to 60 °C. Subsequently, the flow of a H<sub>2</sub>-Ar mixture (10% H<sub>2</sub> by volume) was switched on, and the catalyst was heated to 700 °C at a rate of 10 °C/min. The H<sub>2</sub> consumption was monitored using a thermal conductivity detector (TCD).

O<sub>2</sub>-TPD analysis was performed using the same apparatus as described for H<sub>2</sub>-TPR. First, 100 mg was pretreated at 300 °C using high-purity He (30 mL/min) for 30 min and then cooled to 60 °C. Subsequently, the flow of an O<sub>2</sub>-He mixture (5% O<sub>2</sub> by volume) was switched for 60 min. High-purity He was then switched on, and the system was allowed to stabilize. The sample was heated up to 800 °C at a rate of 10 °C/min. The experiment without O<sub>2</sub> pre-adsorption was performed as above except that the procedure for O<sub>2</sub>-He adsorption was omitted.

### 3. Results

#### 3.1. Toluene decomposition performance

##### 3.1.1. Toluene removal characteristics

Fig. 2 showed the dependence of the toluene removal efficiency on O<sub>2</sub> concentrations ranging from 0 to 20% by volume. For the toluene removal by plasma alone, removal efficiency increased

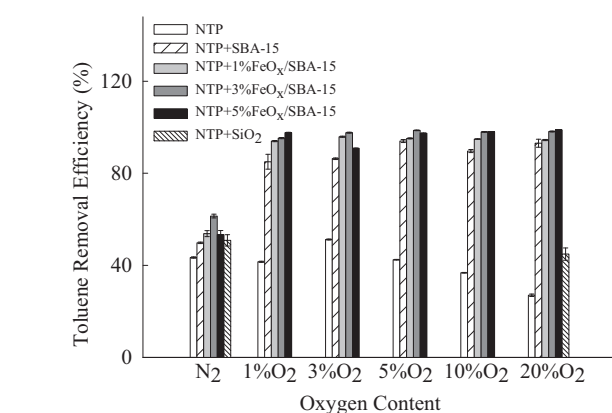


**Fig. 2.** Effect of O<sub>2</sub> concentration on toluene removal efficiency. (Initial concentration of toluene: 100 ppm, SED: 192 J/L).

with the increase of oxygen content, reaching a maximum (51%) at 3% O<sub>2</sub>, and then continuously decreased at higher O<sub>2</sub> contents. When various catalysts were packed into the NTP system, the effect of oxygen's electronegative character disappeared, and the toluene removal efficiency was notably increased by SBA-15, SiO<sub>2</sub> and FeO<sub>x</sub>/SBA-15. The extent of improvement was dependent on the amount of iron loading, where that in the packed FeO<sub>x</sub>/SBA-15 reactor was higher than that in the packed SBA-15 or SiO<sub>2</sub> reactor at the various O<sub>2</sub> concentrations.

##### 3.1.2. Selectivity for CO<sub>2</sub> and CO<sub>x</sub>

Fig. 3 showed the selectivity of CO<sub>2</sub> and CO<sub>x</sub> as a function of O<sub>2</sub> concentration with or without the catalyst. For the plasma-alone and plasma-catalysis systems, the selectivity for CO<sub>2</sub> and CO<sub>x</sub> increased with the increase of O<sub>2</sub> concentration. Under the various O<sub>2</sub> concentrations, the catalysts loaded with 1% and 3%Fe assisted the formation of CO<sub>2</sub> and CO<sub>x</sub> and increased selectivity remarkably. In contrast, the SBA-15, SiO<sub>2</sub> and 5%FeO<sub>x</sub>/SBA-15 catalysts did not improve the selectivity of CO<sub>2</sub> and CO<sub>x</sub> at any of the O<sub>2</sub> concentrations. In addition, when the catalysts loaded with 1% or 3%Fe were introduced into the NTP reactor, the proportion of CO<sub>2</sub> in the CO<sub>x</sub> significantly increased, which indicated that complete oxidation of toluene was enhanced. According to the results for toluene removal efficiency and CO<sub>x</sub> selectivity, the 3%Fe loading catalyst showed excellent toluene degradation performance under the various plasma conditions.

##### 3.1.3. Analysis of the toluene oxidation residues

As observed in Fig. 3, a CO<sub>x</sub> selectivity of less than 100% indicated that some unidentified by-products formed in the reactor. Their species was indicated using GC-MS, as presented in Fig. 4. Nine gaseous organic by-products from toluene decomposition by NTP alone were identified, and their abundance decreased with increasing O<sub>2</sub> concentration, suggesting that the CO<sub>x</sub> selectivity increased with increasing O<sub>2</sub> content, consistent with the results of Fig. 3. When SBA-15 was used in the NTP process, the content of some organic by-products, such as benzyl alcohol; formic acid, phenylmethyl ester; acetic acid, phenylmethyl ester; benzenemethanol, 2-nitro-; tetradecane; hexadecane and heptadecane; decreased in the gas phase, even disappearing at O<sub>2</sub> concentration above 5%. At the same time, the abundance of benzaldehyde also decreased under the various plasma conditions. Meanwhile, using the 3%FeO<sub>x</sub>/SBA-15 packing material, the by-product contents further decreased, even disappearing. The toluene concentration in the various toluene oxidation experiment followed the order of NTP > NTP + SBA-15 > NTP + 3%FeO<sub>x</sub>/SBA-15, which agreed with toluene removal efficiency results for the different processes (Fig. 2).

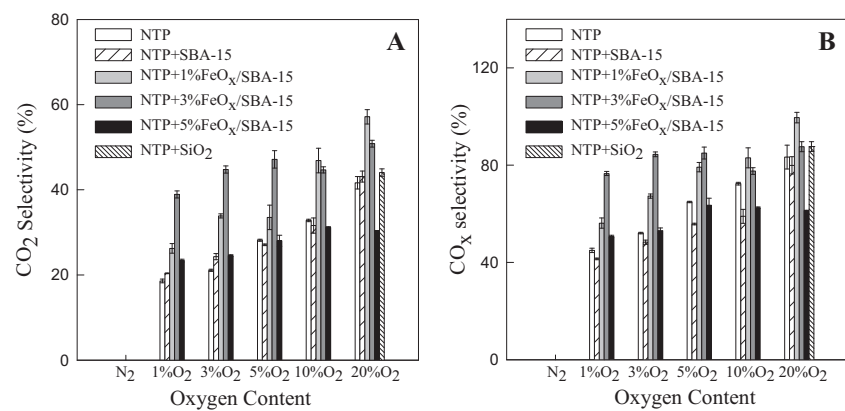


**Fig. 3.** Effect of O<sub>2</sub> concentration on (A) CO<sub>2</sub> selectivity and (B) CO<sub>x</sub> selectivity. (Initial concentration of toluene: 100 ppm, SED: 192 J/L).

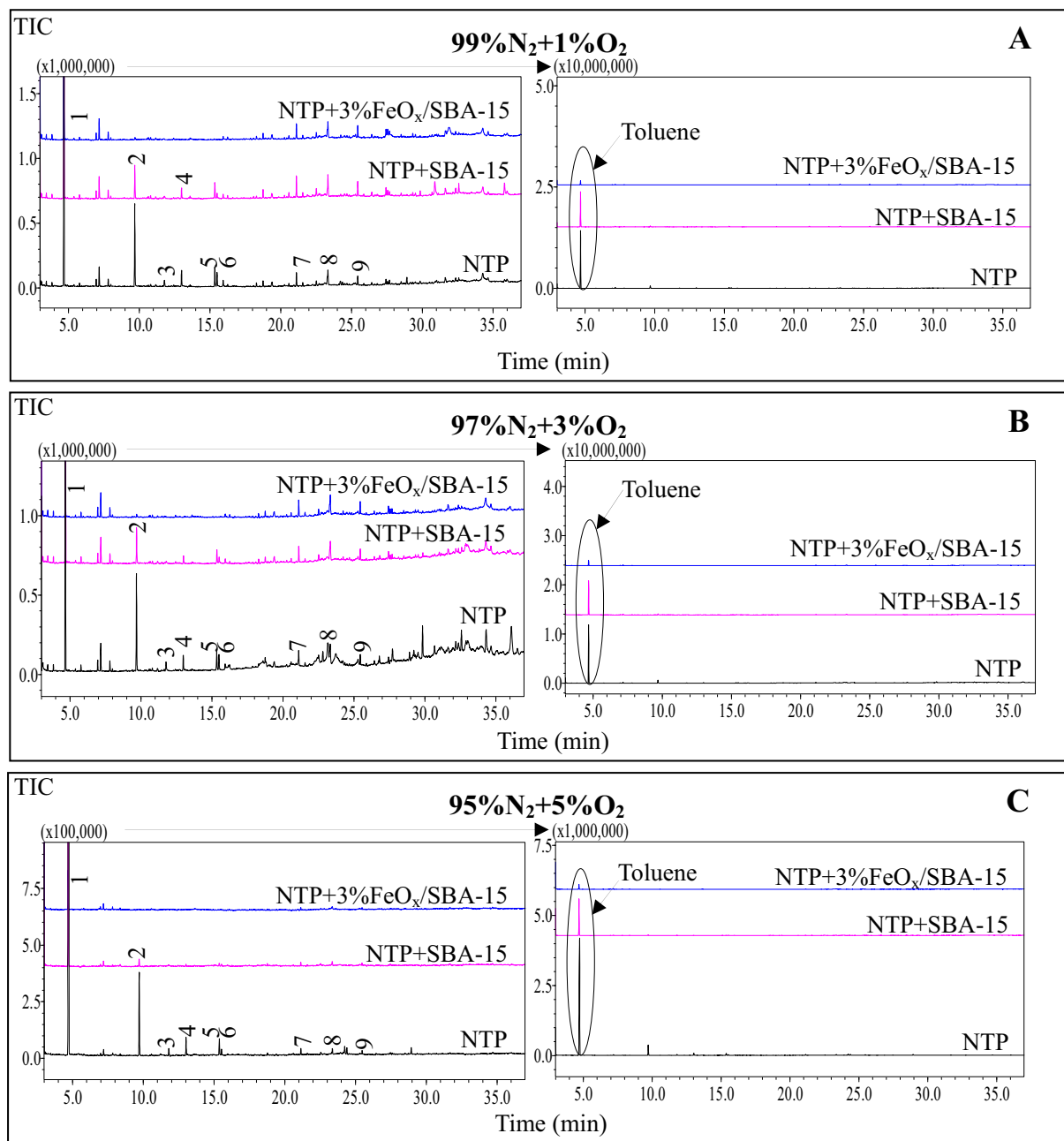
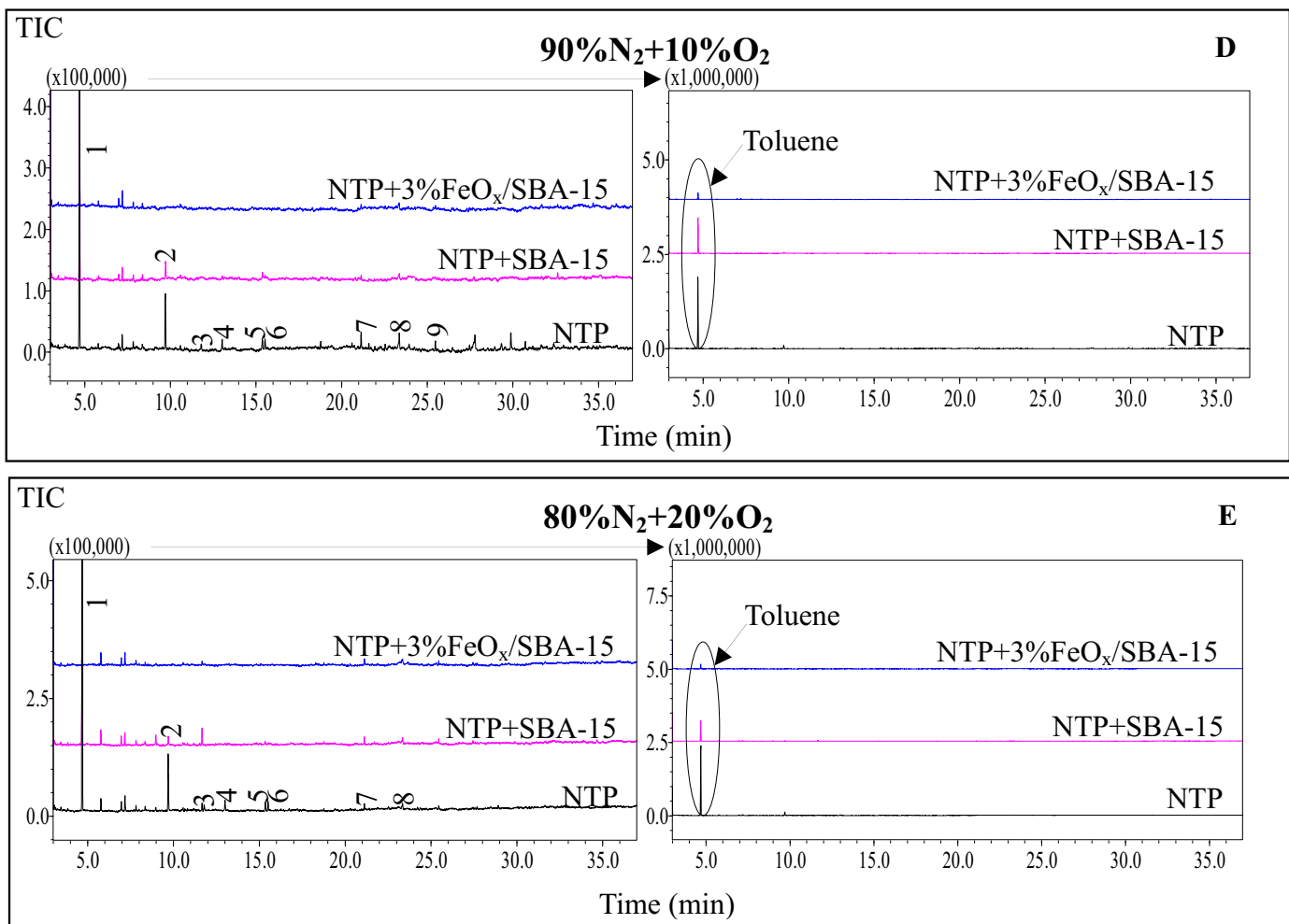


**Fig. 4.** Detailed GC-MS spectrum and identified peaks of organic by-products from toluene decomposition in the gas phase. (Reaction conditions: toluene, 100 ppm; SED, 192 J/L).

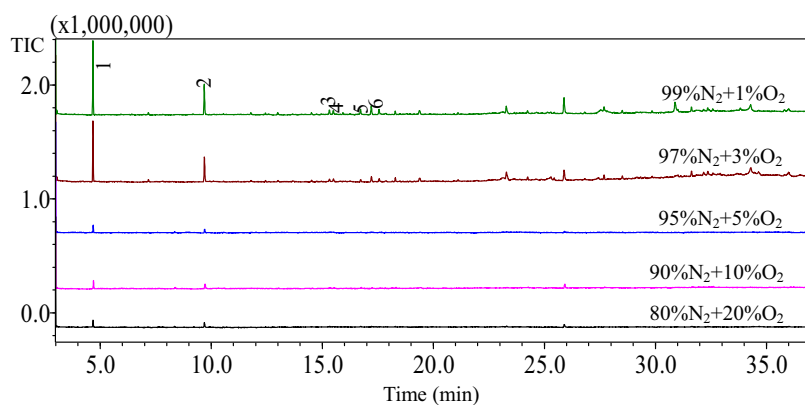


Peak #	Time(min)	Compound name
1	4.67	Toluene
2	9.69	Benzaldehyde
3	11.78	Benzyl alcohol
4	12.98	Formic acid, phenylmethyl ester
5	15.245	Acetic acid, phenylmethyl ester
6	15.495	Benzenemethanol, 2-nitro-
7	21.11	Tetradecane
8	23.34	Hexadecane
9	25.44	Heptadecane

**Fig. 4.** (Continued.)

The organic by-products deposited on the 3%FeO<sub>x</sub>/SBA-15 catalyst surface were also identified (Fig. 5) to obtain a better understanding of the toluene decomposition on the catalyst surface. The number of different by-products decreased as O<sub>2</sub> concentration increased, with only toluene and benzaldehyde being observed in the 80%N<sub>2</sub>+20%O<sub>2</sub> plasma process. In contrast, numerous nitrogen-containing species, such as benzene,

1-methyl-2-nitro-; benzenemethanol,4-nitro-; benzene, 1-methyl-4-nitro-; and phenol,4-methyl-2-nitro-; were identified under the condition of low O<sub>2</sub> concentration. Those species decreased and even vanished with increasing O<sub>2</sub> concentration. During toluene degradation with NTP+3%FeO<sub>x</sub>/SBA-15, the spectrum of toluene emerged on the 3%FeO<sub>x</sub>/SBA-15 surface, and the abundance was higher than that of all of the by-products,



Peak #	Time(min)	Compound name
1	4.67	Toluene
2	9.69	Benzaldehyde
3	15.32	Benzene, 1-methyl-2-nitro-
4	15.495	Benzene-methanol, 4-nitro-
5	16.725	Benzene, 1-methyl-4-nitro-
6	17.205, 17.555	Phenol, 4-methyl-2-nitro-

**Fig. 5.** Detailed GC-MS spectrum and identified peaks of organic by-products from toluene decomposition on the 3%FeO<sub>x</sub>/SBA-15 catalyst surface. (Reaction conditions: toluene, 100 ppm; SED, 192 J/L).

indicating that the toluene could be adsorbed by the catalyst under discharge conditions. Moreover, the benzaldehyde was detected in all of the samples, implying that it was the key intermediate by-product during toluene degradation.

### 3.2. Toluene destruction in the N<sub>2</sub> plasma

Fig. 2 had showed that the toluene removal efficiency was markedly improved by FeO<sub>x</sub>/SBA-15 catalysts in N<sub>2</sub> plasma. To study the influence of the bulk-phase oxygen of the catalyst on the toluene plasma-catalysis oxidation mechanism, the yields of CO<sub>2</sub> and CO in toluene removal with catalyst-assisted N<sub>2</sub> plasma were measured (Fig. 6). As seen, the quantities of CO<sub>2</sub> and CO were related to the iron loading, with the 3%-Fe-loading catalyst exhibiting the highest oxidative activity. The amounts of CO<sub>2</sub> and CO decreased along with the increasing of reaction time, but could still be detected after reaction for 200 min.

Fig. 7 presented the toluene removal efficiency, CO<sub>2</sub> yield and CO yield as a function of SED in the 3%FeO<sub>x</sub>/SBA-15-assisted N<sub>2</sub> plasma process. The results showed that the toluene removal efficiency, CO<sub>2</sub> yield and CO yield increased with the increase of SED, which indicated that the toluene oxidation by the surface oxygen of catalyst was related to the SED. To assess the role of the bulk oxygen of the catalyst in the toluene oxidation, surface oxygen content of the used and fresh catalysts were characterized by XPS (Fig. 8), the data were summarized in Table 1. After the

catalytic test in toluene degradation, the amount of oxygen decreased for the 3%FeO<sub>x</sub>/SBA-15 catalyst but increased for 1%FeO<sub>x</sub>/SBA-15 or 5%FeO<sub>x</sub>/SBA-15 catalyst.

### 3.3. Catalyst characterization

#### 3.3.1. SEM

The catalyst morphology was observed by SEM (Fig. 9). The surface of SBA-15 was very smooth, while some small granules appeared on the iron-loaded SBA-15 surface, and the particle size increased with increased iron loading. The iron oxide particles were evenly dispersed on the SBA-15 surface for the 1%FeO<sub>x</sub>/SBA-15 and 3%FeO<sub>x</sub>/SBA-15 samples but aggregated when the iron loading exceeded 3% (Fig. 9D).

#### 3.3.2. Pore texture and XRD

The pore textures of the FeO<sub>x</sub>/SBA-15 catalysts were presented in Table 2. As seen, the surface area, pore volume and pore diameter were decreased by the iron loading (except the 1% iron loading), and the extent of the decrease increased with increasing iron loading. However, three well-resolved peaks (100), (110) and (200) typical of hexagonal SBA-15, mesoporous silica [21,36], were clearly identified in all of the catalysts (Fig. 10A), which indicated that the highly ordered structure of SBA-15 was retained in the iron loading process. No obvious iron oxide diffraction peaks were observed in the wide-angle range for the 1% iron loading sample (Fig. 10B), while Fe<sub>2</sub>O<sub>3</sub> and Fe<sub>3</sub>O<sub>4</sub> diffraction peaks appeared for the

**Table 1**

Oxygen content on the surfaces of the fresh catalysts and those used in N<sub>2</sub> plasma process as obtained via XPS.

Catalyst	SED (J/L)	Fresh (at.%)	Used (at.%)
SBA-15	192	74.94%	74.43%
1%FeO <sub>x</sub> /SBA-15	192	73.98%	74.29%
3%FeO <sub>x</sub> /SBA-15	122	73.56%	73.35%
	192		72.66%
	284		73.33%
5%FeO <sub>x</sub> /SBA-15	192	73.24%	74.10%

**Table 2**

Surface area, pore diameter and pore volume of different FeO<sub>x</sub>/SBA-15 catalysts.

Catalyst	Surface area (m <sup>2</sup> /g)	Pore volume (cm <sup>3</sup> /g)	Pore diameters (nm)
SBA-15	508	0.85	6.7
1%FeO <sub>x</sub> /SBA-15	518	0.84	6.5
3%FeO <sub>x</sub> /SBA-15	496	0.81	6.5
5%FeO <sub>x</sub> /SBA-15	486	0.78	6.4

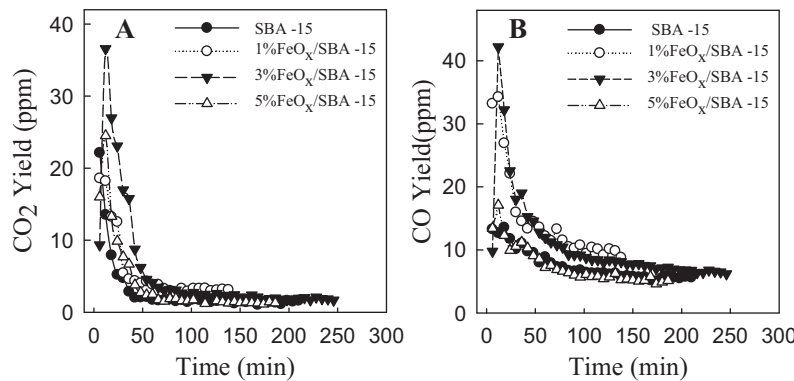


**Fig. 6.** (A) CO<sub>2</sub> and (B) CO yields in toluene removal using the catalysts-assisted N<sub>2</sub> plasma process. (Initial concentration of toluene: 100 ppm, SED: 192 J/L).

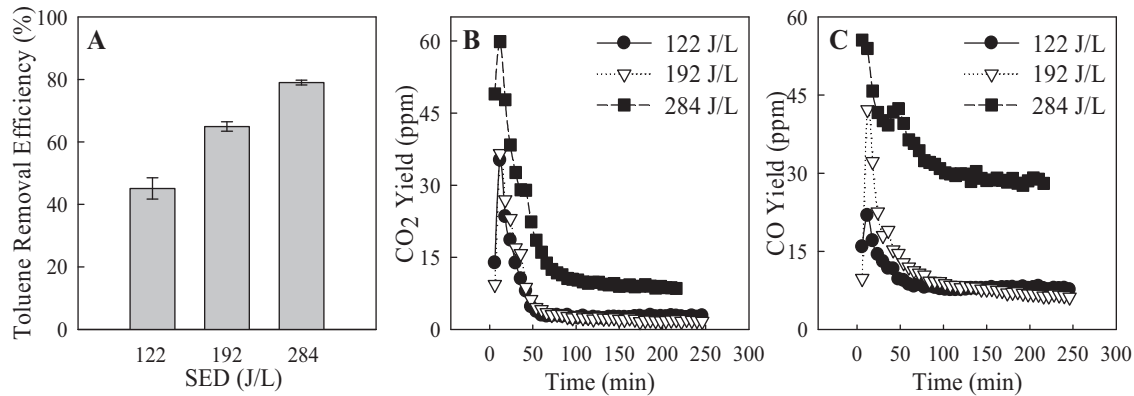


**Fig. 7.** The effect of SED on (A) toluene removal efficiency, (B) CO<sub>2</sub> yield and (C) CO yield in the 3%FeO<sub>x</sub>/SBA-15-assisted N<sub>2</sub> plasma process. (Initial concentration of toluene: 100 ppm).

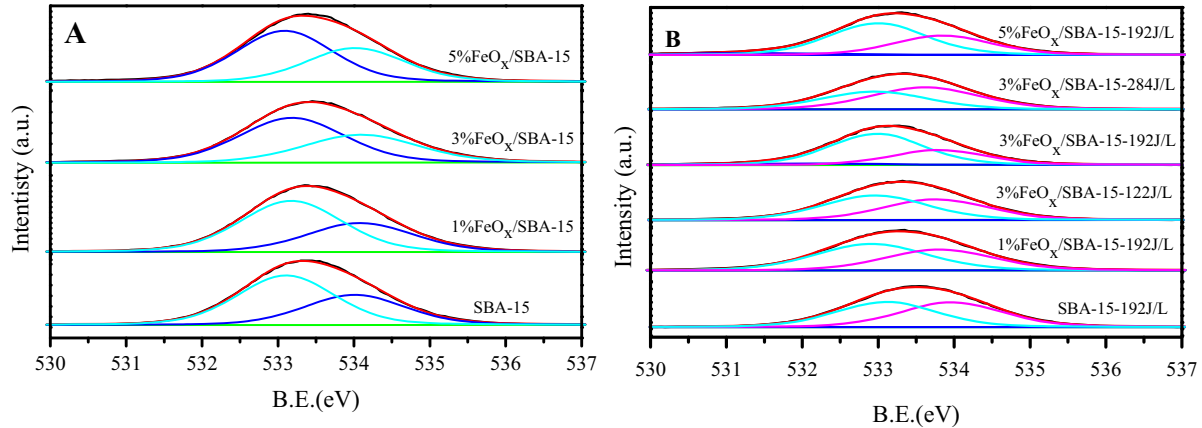


**Fig. 8.** O 1s core level XPS spectra of catalysts: (A) fresh catalyst, (B) used catalyst in the N<sub>2</sub> plasma.

3%- and 5%-Fe-loading catalysts, demonstrating the formation of crystalline Fe<sub>2</sub>O<sub>3</sub> and Fe<sub>3</sub>O<sub>4</sub> on SBA-15 surface with increasing iron loading.

### 3.3.3. XPS

The oxidation states and iron content in the near-surface region were measured using XPS (Fig. 11, Table 3). According to the XPS spectra for Fe 2p (Fig. 11), the binding energies of 710.9–711.6 eV and 712.5–714.4 eV could be ascribed to the presence of Fe<sup>2+</sup> and Fe<sup>3+</sup> species, respectively. The relative percentages of each species were summarized in Table 3. Quantitatively, it was found that the Fe<sup>2+</sup> and Fe<sup>3+</sup> content on the catalyst surface changed as the iron loading increased. The highest Fe<sup>2+</sup> content and lowest Fe<sup>3+</sup> content

was found for the 3%-Fe-loading catalyst, which also had the best performance for toluene oxidation under the plasma conditions, suggesting that the oxidation states of iron played a crucial role in the toluene degradation.

**Table 3**

Atomic surface compositions of the FeO<sub>x</sub>/SBA-15 catalysts obtained via XPS.

Catalyst	Atomic composition (%)			Fe (%)	
	Si	O	Fe	Fe <sup>3+</sup>	Fe <sup>2+</sup>
SBA-15	25.06	74.94			
1%FeO <sub>x</sub> /SBA-15	25.42	73.98	0.60	44.26	55.74
3%FeO <sub>x</sub> /SBA-15	25.74	73.56	0.70	37.02	62.98
5%FeO <sub>x</sub> /SBA-15	25.44	73.24	1.32	70.08	29.92

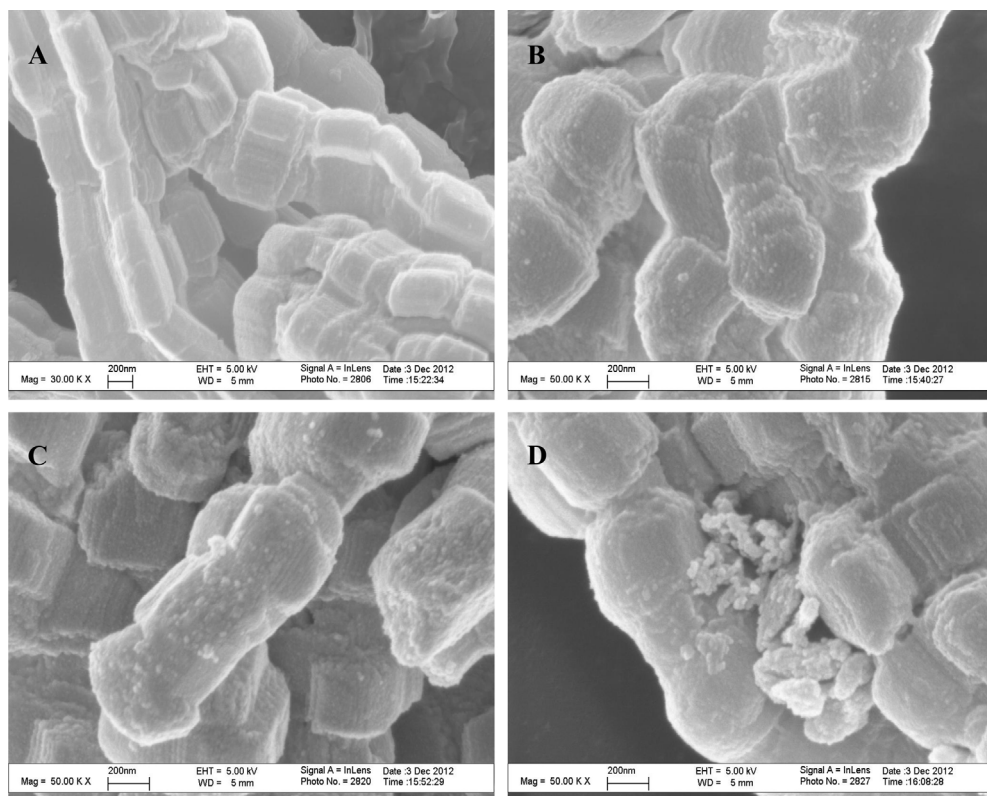


**Fig. 9.** SEM images of various catalysts: (A) SBA-15, (B) 1%FeO<sub>x</sub>/SBA-15, (C) 3%FeO<sub>x</sub>/SBA-15, (D) 5%FeO<sub>x</sub>/SBA-15.

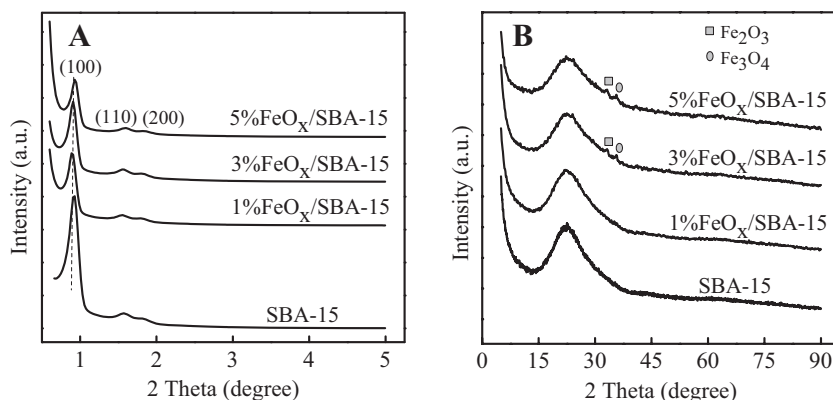


**Fig. 10.** The low-angle (A) and wide-angle (B) XRD patterns of different FeO<sub>x</sub>/SBA-15 catalysts.

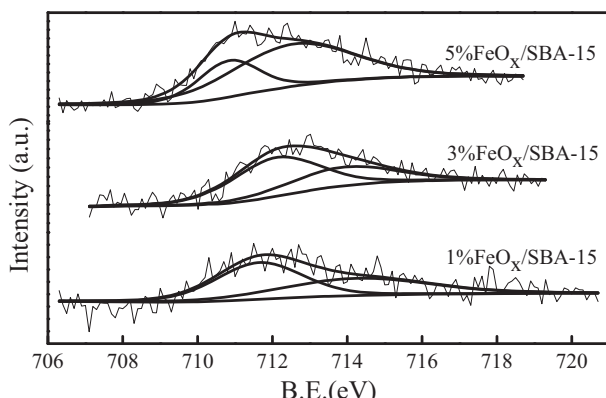


**Fig. 11.** Fe 2p core level XPS spectra of FeO<sub>x</sub>/SBA-15 catalysts.

### 3.3.4. H<sub>2</sub>-TPR

The catalytic properties of FeO<sub>x</sub>/SBA-15 could be determined by the reducibility, which was measured by H<sub>2</sub>-TPR. In the TPR curves of the Fe-loaded catalysts (Fig. 12), the low-temperature reduction peak was centered at 342 °C with a shoulder peak at 492 °C, which could be attributed to the reduction of Fe<sub>2</sub>O<sub>3</sub> → Fe<sub>3</sub>O<sub>4</sub> → Fe [21]. Another shoulder peak at 585 °C or 602 °C appeared with increasing Fe loading and was ascribed to the reduction of Fe<sup>2+</sup> to Fe<sup>0</sup> [37]. Moreover, the temperature of Fe<sup>2+</sup> reduction decreased slightly with increasing iron loading, being lowest for the 3%-Fe-loading catalyst, and then increased as the Fe loading increased further. Quantitative evaluation of the reduction peaks (Table 4), which could be ascribed to the catalyst active center, revealed that the hydrogen consumption increased with increasing Fe loading. However, the best performance of toluene oxidation was achieved using the 3%-Fe-loading catalyst. These findings indicated that the catalyst performance was not exclusively determined by the active

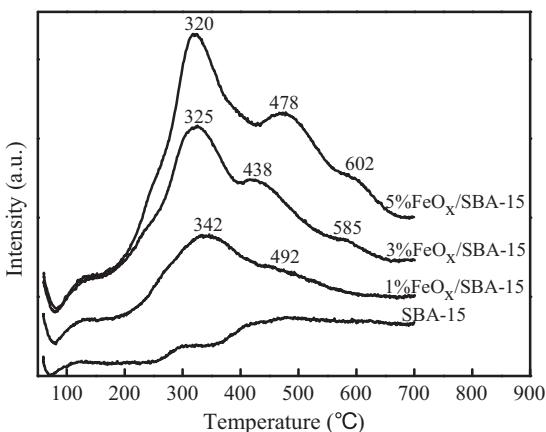


Fig. 12.  $\text{H}_2$ -TPR profiles of various  $\text{FeO}_x/\text{SBA-15}$  catalysts.

**Table 4**  
 $\text{H}_2$  consumption of various catalysts.

Catalyst	$T_1$ ( $^{\circ}\text{C}$ )	$T_2$ ( $^{\circ}\text{C}$ )	$T_3$ ( $^{\circ}\text{C}$ )	Total $\text{H}_2$ (mmol/g)
SBA-15	–	–	–	–
1% $\text{FeO}_x/\text{SBA-15}$	342	492	–	0.66
3% $\text{FeO}_x/\text{SBA-15}$	325	438	585	1.30
5% $\text{FeO}_x/\text{SBA-15}$	320	478	602	2.18

center, as the more active centers were present, the stronger the interaction between the active ingredient and carrier.

### 3.3.5. $\text{O}_2$ -TPD

$\text{O}_2$ -TPD is often used to identify the oxygen species in a catalyst. Various oxygen species could be identified in the catalysts (Fig. 13). The peaks at  $80^{\circ}\text{C}$ ,  $370^{\circ}\text{C}$  and  $>500^{\circ}\text{C}$  were ascribed to the desorption of weak adsorption molecular oxygen ( $\text{O}_2^-$ ), chemically adsorbed oxygen ( $\text{O}^-$ ) and lattice oxygen ( $\text{O}^{2-}$ ), respectively, from the catalyst surface [38,39]. To study the role of iron in the oxygen adsorption,  $\text{O}_2$ -TPD was measured in another way (without the  $\text{O}_2$  adsorption procedure). It was found that the extent of oxygen desorption, especially that of  $\text{O}_2^-$ , significantly increased after iron loading, which revealed that the oxygen adsorption on the catalyst was promoted by iron loading. Meanwhile, the desorption temperature of  $\text{O}^{2-}$  was lower for the case of  $\text{O}_2$  pre-adsorption than for the case without it, implying the improvement of lattice oxygen activity by adsorbed oxygen, which was beneficial for the complete oxidation of toluene.

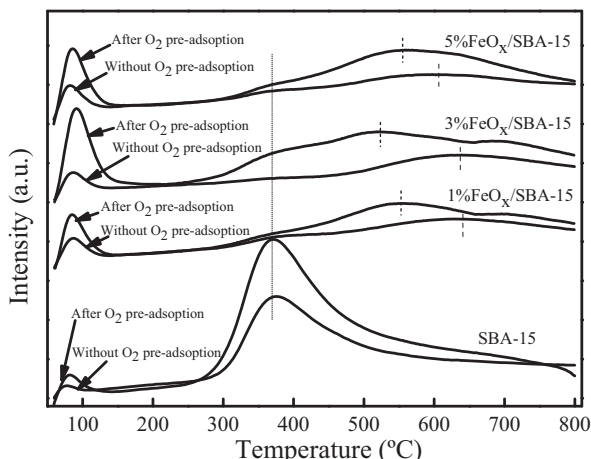


Fig. 13.  $\text{O}_2$ -TPD profiles of various  $\text{FeO}_x/\text{SBA-15}$  catalysts.

### 3.4. Evaluation of catalyst stability

The stability of 3% $\text{FeO}_x/\text{SBA-15}$  catalyst under condition of toluene plasma-catalytic oxidation was assessed with experiments at room temperature and atmospheric pressure. It could be observed that toluene removal proceeded stably during the first 12 h, after which the toluene removal efficiency decreased (Fig. 14A). This observation indicated that the catalyst suffered slight deactivation during prolonged toluene oxidation. However, after the catalytic test (39 h) in toluene plasma-catalytic oxidation, no disruption of 2D-hexagonal structure or phase change was observed in the XRD analysis of the catalysts, because the three typical peaks  $\{(1\ 0\ 0), (1\ 1\ 0), (2\ 0\ 0)\}$  were clearly identified (Fig. 14B), and no new iron diffraction peak was appeared (Fig. 14C).

## 4. Discussion

The dispersion of metal particles on the support was usually correlated with the catalytic activity of a metal catalyst. From the SEM and XRD results, it was known that the  $\text{FeO}_x$  could be highly dispersed on the SBA-15 surface at lower loading. The particle size increased with the iron loading, and aggregation was observed at a loading of 5%Fe, which might depress the adsorption of toluene on the catalyst. From the adsorption breakthrough curves of toluene over different catalysts (Fig. 15), the toluene adsorption ability decreased with increasing of Fe loading, and the SBA-15 showed the best performance. Consequently, the residence time of toluene in the DBD reactor could increase because of the sorption of SBA-15. According to previous literature [17], the increasing of residence time could improve the VOCs removal efficiency. Thus, the toluene adsorption over the SBA-15 could be explained one reason of toluene removal. In order to further study the effect of catalyst adsorption on the toluene removal, experiment of toluene removal by coupling  $\text{SiO}_2$  with NTP system was carried out (Figs. 2 and 3). Although the toluene removal efficiency was greatly increased in comparison with NTP alone, the  $\text{CO}_2$  selectivity and  $\text{CO}_x$  selectivity had no significant increase. Compared with SBA-15-assisted NTP process, the toluene removal efficiency in  $\text{SiO}_2$ -assisted NTP process was not improved in the environment of 100% $\text{N}_2$  plasma and even decreased under the condition of 80% $\text{N}_2$  + 20% $\text{O}_2$  plasma. And from the adsorption breakthrough curves of toluene over  $\text{SiO}_2$ , we could know that it had not the capability of toluene adsorption (Fig. 15). These results further suggested that the toluene adsorption over catalyst played an important role in the plasma catalysis system.

Additionally, it was interesting to observe that the  $\text{CO}_x$  selectivity using  $\text{FeO}_x/\text{SBA-15}$  in DBD reactor was much higher than that using pure SBA-15. This phenomenon was probable due to the excellent oxygen-supplying ability of  $\text{FeO}_x$ , which had been suggested in the process of toluene  $\text{N}_2$  plasma-catalytic oxidation (Fig. 6). Previous studies revealed that VOC removal was better catalyzed using mainly catalysts ( $\text{TiO}_2$ ,  $\gamma$ - $\text{Al}_2\text{O}_3$ , zeolites) rather than supported metal catalysts [28,40]. However, in our study, the interaction of  $\text{FeO}_x$  and SBA-15 was found to play an important role in toluene removal using the combination of  $\text{FeO}_x/\text{SBA-15}$  with plasma. The stability of catalyst 3% $\text{FeO}_x/\text{SBA-15}$  was also studied (Fig. 14), despite slight deactivation during prolonged toluene oxidation reaction, the structure of the catalyst was perfectly stable over the period of 39 h for 100 ppm of toluene plasma-catalysis oxidation, and no active component run off was detected. So the activity of the catalyst could be recovered through the appropriate method.

The influence of oxygen on VOC removal has been extensively studied, revealing that the maximum VOC decomposition efficiency occurred at a given oxygen content, for example, 5% for toluene

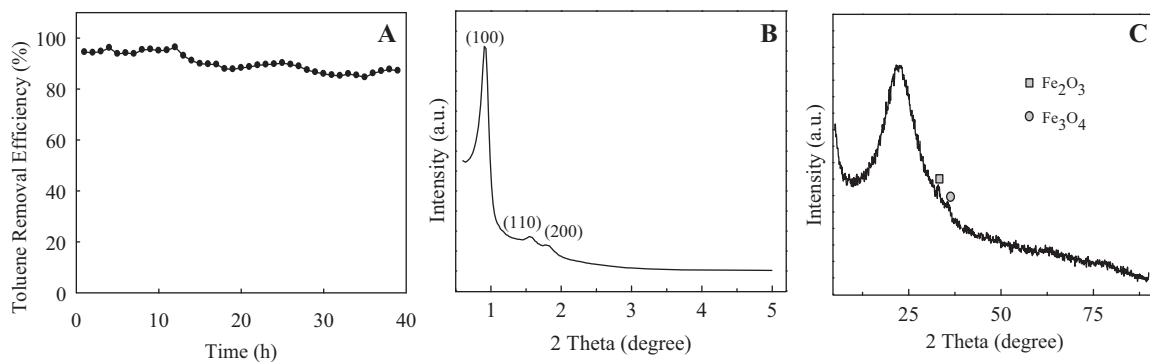


**Fig. 14.** (A) Toluene removal over catalyst as a function of time, (B) low-angle and (C) wide-angle XRD patterns of catalyst after 39 h catalytic test. (Catalyst: 3% $\text{FeO}_x$ /SBA-15; initial concentration of toluene: 100 ppm, feed gas: 80% $\text{N}_2$  + 20% $\text{O}_2$ , SED: 192 J/L).

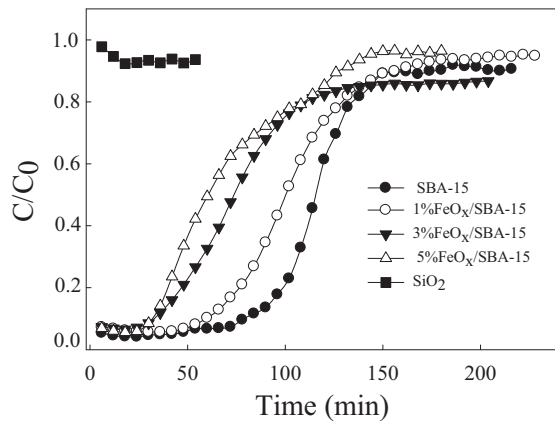
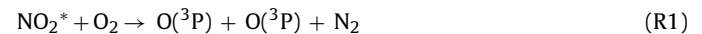


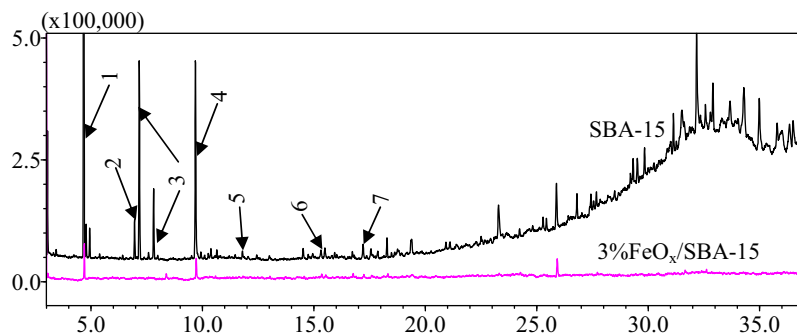
**Fig. 15.** Adsorption breakthrough curves of toluene over different catalysts.

[41], 20% for  $\text{CF}_4$  [42] and 10% for  $\text{C}_2\text{F}_6$  [8]. We found the maximum toluene removal efficiency at 3% (Fig. 2). The differences between these results were attributed to the difference in the experimental conditions. The VOCs could be destroyed by collision with the

nitrogen excited species, especially the metastable states of nitrogen molecules ( $\text{N}_2(\text{A}^3\Sigma_u^+)$ ), which were considered an energy reservoir [43–45]. Correspondingly, some nitrogen-containing species were identified in the gas phase and on the catalyst surface (Figs. 4 and 5). On the other hand, oxygen excited species could also be formed in the case of a gas stream containing oxygen. Such species demonstrated higher oxidizability for VOCs, resulting in a decrease in organic by-products and an increase in the toluene removal efficiency with increasing oxygen content. However, a lower toluene destruction efficiency was found in higher-oxygen-content gas. This finding could be attributed to the electronegativity of the oxygen molecules and the decrease in the oxygen excited species due to the quenching of the high-energy ions (R1) [43–46].



It had been widely accepted that the loading amount of the active component and the oxidation states were important factors that determine VOC oxidation. Iron usually exists as  $\text{Fe}^{2+}$  and  $\text{Fe}^{3+}$  in oxide, and could transport  $\text{O}_2$  via interconversion between  $\text{Fe}^{2+}$  and  $\text{Fe}^{3+}$  [24]. As seen from the XPS results (Fig. 11 and Table 3), the  $\text{Fe}^{2+}$  content was the highest for the 3%-Fe-loading catalyst,



Peak #	Time(min)	Compound name
1	4.67	Toluene
2	6.96	Ethybenzene
3	7.17, 7.81	o-xylene, p-xylene
4	9.69	Benzaldehyde
5	11.78	Benzyl alcohol
6	15.32	Benzene, 1-methyl-2-nitro-
7	17.205	Phenol,4-methyl-2-nitro-

**Fig. 16.** GC-MS chromatogram of the organic by-products of toluene decomposition on the catalyst surface. (Reaction condition: toluene, 100 ppm; feed gas, 90% $\text{N}_2$  + 10% $\text{O}_2$ ; SED, 192 J/L).

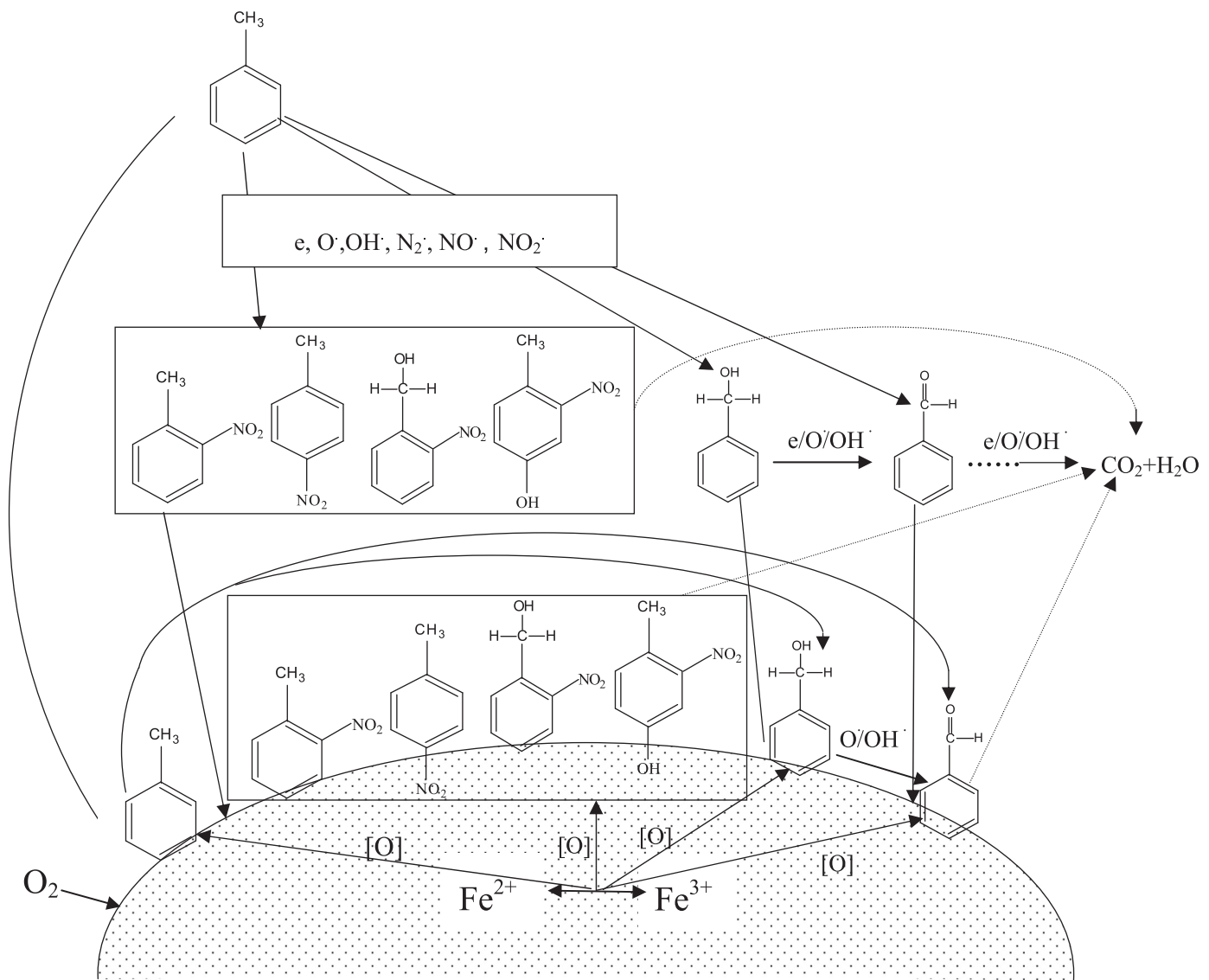
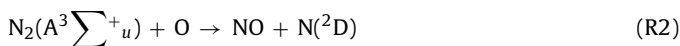


**Fig. 17.** Pathways of toluene degradation in the gas phase and on the FeO<sub>x</sub>/SBA-15 surface.

which had the best catalytic performance. Thus, the Fe<sup>2+</sup> content might play a vital role in the destruction of toluene molecules in the FeO<sub>x</sub>/SBA-15-catalyst-assisted plasma system. As is known, Fe<sup>3+</sup> has a better deoxidation capability because of its lower reduction temperature (Fig. 12). The catalyst with 5%Fe loading had the highest content of Fe<sup>3+</sup>, but its catalytic activity toward toluene was poor due to the stronger interaction of FeO<sub>x</sub> with the support (Table 4). This further demonstrated that FeO<sub>x</sub> and SBA-15 both played important roles in the toluene oxidation. In terms of the O<sub>2</sub>-TPD results, it was found that iron loading increased the oxygen adsorption, especially that of the molecular oxygen on the catalyst surface. Because of this characteristic, the oxygen could transfer from the gas phase to the catalyst surface, consequently decreased the O<sub>2</sub> electronegative characteristics in the gas phase. Moreover, after oxygen adsorption over the catalyst surface, the oxygen consumption (as follows (R2)–(R4) [43]), could also decrease.



Therefore, Fe loading improved the utilization efficiency of active oxygen. Meanwhile, we also found that the adsorbed oxygen improved the activity of lattice oxygen (Fig. 13), which was favorable for the toluene complete oxidation [47].

It had been reported that bulk-phase oxygen species were key factors for the oxidation activity of metal oxide catalysts [48]. Reactions without oxygen in the feed were performed for toluene oxidation at room temperature. As expected, the oxidation of toluene over the various FeO<sub>x</sub> catalysts occurred in the absence of any gaseous oxygen (Figs. 6 and 7), which was in agreement with the results reported by Ogata [31] and Futamura [49]. It is known that electrical discharge is an effective mechanism for activating gas-phase oxygen. The higher the applied voltage, the more high-energy electrons, atoms, ions, free radicals and excited species are created [43], which were beneficial for the catalyst activation [50]. Thus, the yields of CO<sub>2</sub> and CO in the N<sub>2</sub> plasma process increased with increasing SED (Fig. 7B and C). It should also be noted that a large amount of sub-surface oxygen was present in the catalyst. During toluene oxidation, this oxygen could move to the catalyst surface [51], resulting in the observation of CO<sub>x</sub> after 3 h of the reaction had passed. In addition, the bulk-oxygen in the 1% or 5%Fe-loading catalyst could not quickly react with the VOCs adsorbed on

the catalyst surface, resulting in an increase in the oxygen content of the sample after reaction (Table 1). These observations suggested that the bulk-phase oxygen of the 3%FeO<sub>x</sub> catalyst might be more easily activated by plasma than that of other catalysts.

Different pathways for VOC decomposition by NTP had been proposed according to the identified intermediates in previous studies [13,43,52]. However, most studies focused on the pathways in the gas phase. In this study, possible pathways at the interface between the gas phase and catalyst were relevant, which were scarce in the literature. As can be seen in Fig. 4, the Fe loading markedly decreased the number of species and the concentration of organic by-products. To study the influence of Fe loading on the toluene oxidation over the catalyst, an additional experiment was carried out with 3%FeO<sub>x</sub>/SBA-15 and pure SBA-15 in a 90%N<sub>2</sub>+10%O<sub>2</sub> feed gas (Fig. 16). Compared to SBA-15, the number of species and the concentration of the by-products were remarkably decreased for the catalyst with 3% FeO<sub>x</sub> loading, and no nitrogen-containing intermediates, ethybenzene and xylene were observed. This finding indicated that Fe loading promoted the deep oxidation of toluene, forming more CO<sub>2</sub> and CO and thereby increasing the CO<sub>2</sub> and CO<sub>x</sub> selectivity (Fig. 3). Another hand, the content of some organic by-products in the gas phase was also decreased by the SBA-15 (Fig. 4), while the CO and CO<sub>2</sub> selectivity were not improved by it (Fig. 3). Thus, the benefits of utilization of SBA-15 in this system might be considered to adsorb or incompletely oxidize for the toluene.

Thus, based on the organic by-products of toluene decomposition in the gas phase and on the catalyst surface, the following toluene oxidation mechanism was proposed, as shown in Fig. 17. The principle processes of toluene destruction were induced by energetic electrons, active oxygen species as well as hydroxyl and nitrogen excited species in the reactor. The tentative reaction scheme included two parts: a reaction in the gas phase, namely, the direct removal caused by the collision of electrons or oxidation caused by the gas-phase radicals (O<sub>•</sub>, OH<sub>•</sub>, N<sub>2</sub>O<sub>•</sub>, NO<sub>•</sub>, NO<sub>2</sub>O<sub>•</sub>), and a reaction on the catalyst surface, namely, the reaction between adsorbed toluene or other intermediate by-products (such as benzaldehyde, benzyl alcohol and nitrogen-containing intermediates) and the active species (such as O<sub>•</sub> and OH<sub>•</sub>). Moreover, the O<sub>2</sub> in the gas stream might be fixed on the catalyst surface via facile interconversion between Fe<sup>2+</sup> and Fe<sup>3+</sup> states and then be transported to the toluene or intermediate organic by-products over the catalyst, leading to the formation of CO<sub>2</sub>. As known, an opening of the aromatic ring happened both in gas-phase and on catalyst surface [13,14], and then a series of oxidations of the aromatic ring steps could take place. While no opening of the aromatic ring intermediates were identified in this study. Thus, we discussed only a conceivable pathway that was operative in the gas-phase and on the catalyst surface based on the results from the GC-MS, the pathways of CO<sub>x</sub> formation from toluene derivatives was not discussed in this study.

## 5. Conclusions

The combination of the FeO<sub>x</sub>/SBA-15 catalyst with NTP greatly increased the toluene removal efficiency and CO<sub>x</sub> selectivity and markedly reduced the production of organic intermediates. Optimal toluene oxidation was achieved with 3% Fe loading, which was closely related to the highly dispersed nature of 3% FeO<sub>x</sub> on the SBA-15 surface, the relatively low reduction temperature of Fe<sup>2+</sup> and its excellent oxygen adsorption ability. The toluene destruction test in pure N<sub>2</sub> plasma indicated that the bulk-oxygen in the catalyst was involved in the toluene oxidation, and the degree of toluene oxidation increased with increasing SED. The toluene removal depended on two pathway: (1) direct degradation in the gas phase caused by

the collision of electrons or oxidation and (2) the reaction on the catalyst surface caused by the oxidation of active species (such as O<sub>•</sub> and OH<sub>•</sub>). Among the multiple oxidation processes in the coupled FeO<sub>x</sub>/SBA-15 and NTP system, the Fe<sup>2+</sup> was considered to be an important contributor because of its outstanding O<sub>2</sub> adsorption ability. SBA-15 also played an important role because of its excellent toluene adsorption ability.

## Acknowledgments

We would like to thank Hangao Liu and Peitao Wang for helping us to build experimental system. Thanks Mr. Don Barnes, Prof. Shiming Luo, Dr. Shafiq UR Rehman, and Dr. Yanxia Su for valuable suggestions and English check. This work was carried out with the supported of “the National Natural Science Foundation of China (no. 50978103, no. U1201231, no. 51108187 and no. 51378218)”.

## References

- [1] A.M. Vandenbroucke, R. Morent, N. De Geyter, C. Leys, J. Hazard. Mater. 195 (2011) 30–54.
- [2] S. Schmid, M.C. Jecklin, R. Zenobi, Chemosphere 79 (2010) 124–130.
- [3] N. Harada, T. Matsuyama, H. Yamamoto, J. Electrostat. 65 (2007) 43–53.
- [4] N. Jiang, N. Lu, J. Li, Y. Wu, Plasma Sci. Technol. 14 (2012) 140–146.
- [5] W. Mista, R. Kacprzyk, Catal. Today 137 (2008) 345–349.
- [6] J. Van Durme, J. Dewulf, W. Sysmans, C. Leys, H. Van Langenhove, Chemosphere 68 (2007) 1821–1829.
- [7] M. Magureanu, N.B. Mandache, V.I. Parvulescu, C. Subrahmanyam, A. Renken, L. Kiwi-Minsker, Appl. Catal. B: Environ. 74 (2007) 270–277.
- [8] M.B. Chang, S.J. Yu, Environ. Sci. Technol. 35 (2001) 1587–1592.
- [9] D.Z. Zhao, X.S. Li, C. Shi, H.Y. Fan, A.M. Zhu, Chem. Eng. Sci. 66 (2011) 3922–3929.
- [10] Narengerile, T. Watanabe, Chem. Eng. Sci. 69 (2012) 296–303.
- [11] H. Wang, D. Li, Y. Wu, J. Li, G. Li, J. Electrostat. 67 (2009) 547–553.
- [12] M.S. Gandhi, A. Ananth, Y.S. Mok, J.-I. Song, K.-H. Park, Chemosphere 91 (2013) 685–691.
- [13] W.-J. Liang, L. Ma, H. Liu, J. Li, Chemosphere 92 (2013) 1390–1395.
- [14] H.B. Huang, D.Q. Ye, D.Y.C. Leung, F.D. Feng, X.J. Guan, J. Mol. Catal. A: Chem. 336 (2011) 87–93.
- [15] Y.L. Sun, L.B. Zhou, L.H. Zhang, H. Sui, J. Environ. Sci. 24 (2012) 891–896.
- [16] J. Karuppiah, E. Linga Reddy, P. Manoj Kumar Reddy, B. Ramaraju, R. Karvembu, C. Subrahmanyam, J. Hazard. Mater. 237–238 (2012) 283–289.
- [17] Y.H. Song, S.J. Kim, K.I. Choi, T. Yamamoto, J. Electrostat. 55 (2002) 189–201.
- [18] M.S. Gandhi, A. Ananth, Y.S. Mok, J.-I. Song, K.-H. Park, Res. Chem. Intermed. (2013), <http://dx.doi.org/10.1007/s11164-013-1053-z>.
- [19] H.-H. Kim, M. Sugawara, H. Hirata, Y. Teramoto, K. Kosuge, N. Negishi, A. Ogata, Plasma Chem. Plasma Process. 33 (2013) 1083–1098.
- [20] W.W. Zhang, Z.P. Qu, X.Y. Li, Y. Wang, D. Ma, J.J. Wu, J. Environ. Sci. 24 (2012) 520–528.
- [21] H.L. Zhang, C.J. Tang, C.Z. Sun, L. Qi, F. Gao, L. Dong, Y. Chen, Microporous Mesoporous Mater. 151 (2012) 44–55.
- [22] H.L. Wang, H. Tian, Z.P. Hao, J. Environ. Sci. 24 (2012) 536–540.
- [23] S.C. Kim, W.G. Shim, J. Hazard. Mater. 154 (2008) 310–316.
- [24] Q. Fu, W.-X. Li, Y.X. Yao, H.Y. Liu, H.-Y. Su, D. Ma, X.-K. Gu, L.M. Chen, Z. Wang, H. Zhang, B. Wang, X.H. Bao, Science 328 (2010) 1141–1144.
- [25] X.B. Liao, Y.F. Guo, D.Q. Ye, Acta Sci. Circumstantiae 30 (2010) 1824–1832 (In Chinese with English abstract).
- [26] R. Ono, Y. Yamashita, K. Takezawa, T. Oda, J. Phys. D: Appl. Phys. 38 (2005) 2812.
- [27] S. Choi, S.H. Hong, H.S. Lee, T. Watanabe, Chem. Eng. J. 185–186 (2012) 193–200.
- [28] H.H. Kim, A. Ogata, S. Futamura, Appl. Catal. B: Environ. 79 (2008) 356–367.
- [29] L.S. Wang, B.C. Huang, Y.X. Su, G.Y. Zhou, K.L. Wang, H.C. Luo, D.Q. Ye, Chem. Eng. J. 192 (2012) 232–241.
- [30] H.F. Li, G.Z. Lu, Q.G. Dai, Y.Q. Wang, Y. Guo, Y.L. Guo, Appl. Catal. B: Environ. 102 (2011) 475–483.
- [31] A. Ogata, H.H. Kim, S. Futamura, S. Kusiyama, K. Mizuno, Appl. Catal. B: Environ. 53 (2004) 175–180.
- [32] H.H. Kim, A. Ogata, M. Schiorlin, E. Marotta, C. Paradisi, Catal. Lett. 141 (2011) 277–282.
- [33] X. Yan, T.L. Zhu, X. Fan, Y.F. Sun, Chem. Eng. J. 245 (2014) 41–46.
- [34] J.L. Wu, Q.B. Xia, H.H. Wang, Z. Li, Appl. Catal. B: Environ. 156–157 (2014) 265–272.
- [35] X. Fan, T.L. Zhu, Y.F. Sun, X. Yan, J. Hazard. Mater. 196 (2011) 380–385.
- [36] R.H. Huang, H.H. Yan, L.S. Li, D.Y. Deng, Y.H. Shu, Q.Y. Zhang, Appl. Catal. B: Environ. 106 (2011) 264–271.
- [37] C. Wang, Q.X. Wang, X.D. Sun, L.Y. Xu, Catal. Lett. 105 (2005) 93–101.
- [38] K.Z. Li, H. Wang, Y.G. Wei, M.C. Liu, J. Rare Earths 26 (2008) 705–710.
- [39] C.Y. Ma, W.J. Xue, J.J. Li, W. Xing, Z.P. Hao, Green Chem. 15 (2013) 1035–1041.
- [40] H.H. Kim, A. Ogata, S. Futamura, T. Ieee, Plasma Sci. 34 (2006) 984–995.
- [41] Y.F. Guo, D.Q. Ye, K.F. Chen, J.C. He, W.L. Chen, J. Mol. Catal. A: Chem. 245 (2006) 93–100.
- [42] M.B. Chang, H.M. Lee, Catal. Today 89 (2004) 109–115.

- [43] A.A. Abdelaziz, T. Seto, M. Abdel-Salam, Y. Otani, *J. Hazard. Mater.* 246–247 (2013) 26–33.
- [44] N. Blin-Simiand, S. Pasquier, F. Jorand, C. Postel, J.-R. Vacher, *J. Phys. D: Appl. Phys.* 42 (2009) 122003.
- [45] L. Yu, X. Tu, X.D. Li, Y. Wang, Y. Chi, J.H. Yan, *J. Hazard. Mater.* 180 (2010) 449–455.
- [46] H.M. Lee, M.B. Chang, *Plasma Chem. Plasma Process.* 21 (2001) 329–343.
- [47] H.Q. Lu, L. Shi, C. He, W.Z. Wang, C.J. Huang, H.L. Wan, *Acta Phys. Chim. Sin.* 28 (2012) 2697–2704 (In Chinese with English abstract).
- [48] V.P. Santos, M.F.R. Pereira, J.J.M. Órfão, J.L. Figueiredo, *Appl. Catal. B: Environ.* 99 (2010) 353–363.
- [49] S. Futamura, A.H. Zhang, T. Yamamoto, *J. Electrostat.* 42 (1997) 51–62.
- [50] H.L. Chen, H.M. Lee, S.H. Chen, Y. Chao, M.B. Chang, *Appl. Catal. B: Environ.* 85 (2008) 1–9.
- [51] R.J. Li, S.K. Shen, *J. Mol. Catal. (China)* 15 (2001) 181–186 (In Chinese with English abstract).
- [52] W.F.L.M. Hoeben, F.J.C.M. Beckers, A.J.M. Pemen, E.J.M. van Heesch, W.L. Kling, *J. Phys. D: Appl. Phys.* 45 (2012) 1–14.